Journal of
Applied Crystallography
ISSN 0021-8898

Received 16 August 2006
Accepted 26 February 2007

Multiple-length-scale small-angle X-ray scattering analysis on maghemite nanocomposites

Angel Millan,[a]* Ainhoa Urtizberea,[a] Nuno Joao de Oliveira Silva,[b] Peter Boesecke,[c] Eva Natividad,[a] Fernando Palacio,[a] Etienne Snoeck,[d] Leonardo Soriano,[e] Alejandro Gutiérrez[e] and Carlos Quirós[f]

[a]Instituto de Ciencia de Materiales de Aragón, Spain, [b]Departamento de Física, Universidade de Aveiro, Portugal, [c]European Synchrotron Radiation Facility, BP 220, 38043 Grenoble Cedex, France, [d]CEMES-CNRS, 29 rue Jeanne Marvig, F-31055 Toulouse Cedex, France, [e]Departamento de Física Aplicada, Universidad Autónoma de Madrid, Madrid, E-28049, Spain, and [f]Departamento de Física, Universidad de Oviedo, Avda. Calvo Sotelo s/n, 33007 Oviedo, Spain. Correspondence e-mail: amillan@unizar.es

Small-angle X-ray scattering (SAXS) analysis has been performed on maghemite–poly(4-vinylpyridine) nanocomposites prepared by *in situ* precipitation from iron–polymer coordination compounds. According to electron microscopy observations, the nanocomposites contain isolated spherical particles with a narrow size distribution, uniformly distributed throughout the polymer matrix. The scattering intensity of nanocomposites has relevant contributions from both the polymer and the nanocomposites, showing features characteristic of multiscale structured systems, namely two power laws and a Guinier regime. The data have been analysed in terms of Beaucage's unified approach and it is found that the maghemite particle size increases with the iron/polymer weight ratio used in the preparation of the nanocomposites. SAXS curves also feature a bump that was analysed as arising from a second particle population or from interactions. Magnetization and transmission electron microscopy results give arguments favouring the latter interpretation. It is found that the maghemite particle sizes vary linearly with the iron weight ratio used in the preparation of the nanocomposites.

1. Introduction

Maghemite nanocomposites are interesting in industry, medicine and science. Their main industrial applications include: magnetic recording (Veitch, 2001), printing (Meisen & Kathrein, 2000), sealing (Bhimani & Wilson, 1997), damping (Kamiyama *et al.*, 2002), water purification (Takafuji *et al.*, 2004), sensors (Crainic & Schlett, 2004) and communication (Redl *et al.*, 2003; Chin, 2000). They are particularly attractive in medicine, in the development of novel techniques for early diagnosis (Weissleder & Papisov, 1992), non-invasive therapy (Jordan *et al.*, 2001; Brigger *et al.*, 2002), and biochemical and physiological studies (Bogoyevitch *et al.*, 2002; Uhlen, 1989). In physics, the possibility of controlling interparticle separation allows these materials to be used as model systems for the study of magnetic properties of nanoparticles arising from their finite size and high specific surface (Iglesias & Labarta, 2001). Maghemite nanoparticles are also of great interest in earth and planetary sciences (Schwertmann & Taylor, 1989), and in the life sciences (Safarik & Safarikova, 2002). The interest of magnetic nanocomposites is based on their unique properties, such as superparamagnetism, giant magnetoresistance and magnetic quantum tunnelling, and the ability to modulate their magnetic properties. Other possible advantages associated with their hybrid composition are the combination of organic and inorganic properties in the same compound, and the development of new properties from organic–inorganic synergies. All these properties are very sensitive to particle size and shape (Iglesias & Labarta, 2001), particle–matrix interphases (Brosseau *et al.*, 2003), and interparticle interactions (Mørup & Tronc, 1994). Therefore, a good size characterization for the nanoparticles is a fundamental step in the study of these materials. Small-angle X-ray scattering (SAXS) is an appropriate tool for this characterization. It has been extensively employed in the analysis of nanoparticles dispersions, but not as often for nanocomposite materials. Here, we present results on the SAXS examination of maghemite polymer nanocomposites with several particle sizes and particle densities. The polymer is poly(4-vinylpyridine) (PVP), which can form N–*M* coordination bonds with transition metal ions (Fig. 1). The SAXS curves of nanocomposite pellet samples are compared with those of the pure polymer, pure maghemite powders and as-prepared nanocomposite films. The results are analysed considering electron microscopy observations, X-ray diffraction patterns and magnetic measurements. The SAXS curves show features that can be related to particle surface scattering,

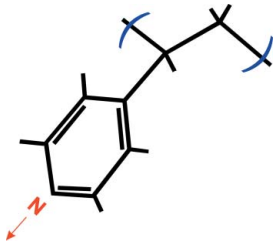

Figure 1
Poly(4-vinylpyridine) polymer.

particle size and nanocomposite structure. The results are interpreted in terms of the Beaucage approach (Beaucage, 1995, 1996; Beaucage *et al.*, 2004).

2. Experimental

2.1. Synthesis of maghemite/poly(4-vinylpyridine) nanocomposites

Maghemite nanoparticles are produced by hydrolysis of iron bromide salts (Millan *et al.*, 2007). Two different iron bromide stock solutions have been used in the synthesis of maghemite nanocomposites. Stock solution 1 contained 1.07 mol dm^{-3} of RbBr and 2.14 mol dm^{-3} of iron bromide, and stock solution 2 contained 0.5 mol dm^{-3} of RbBr and 1 mol dm^{-3} of iron bromide. 35 and 11% of the total iron was in the form of Fe^{II} in stock solutions 1 and 2, respectively. Maghemite powders in aqueous solutions were prepared by addition of 300 cm^3 of 0.1 *M* NaOH to 100 cm^3 of a solution prepared by dilution of 10 cm^3 of stock solution 2, with magnetic stirring, at room temperature. The precipitate was filtered, washed with a saturated sodium oxalate solution and with water, and dried in an oven at 473 K for 24 h. A standard procedure to prepare maghemite/PVP nanocomposites was: a solution of 0.2 g of PVP in 4 cm^3 of a water:acetone (1:1) mixture was mixed with 1 cm^3 of stock solution. The resulting viscous solution was dried in an oven at 313 K for 24 h to obtain a solid film. This film was immersed in 5 cm^3 of a 1 *M* NaOH solution for 1 h, washed with water and dried in an oven at 473 K for 24 h.

2.2. Sample characterization

The materials were characterized by X-ray powder diffraction (XRD) (Rigaku D-max B), transmission electron microscopy (TEM) (Philips CM30, 1.9 Å point resolution), a.c. magnetic measurements (Quantum Design MPMS SQUID magnetometer) and infrared spectroscopy (IR) (Perkin Elmer FT-IR Spectrum One and Perkin Elmer 599 for the far IR).

The nanocomposite samples for SAXS observations were prepared by grinding the as-prepared films in a mortar and then pressing the grains into pellets. Some nanocomposite sample films were observed as prepared. Maghemite pure powder samples were prepared in two ways: (1) by directly pressing the powders into pellets; and (2) by mixing maghemite powders and polymer grains in a mortar and pressing the mixture into pellets. Most of the pellets have a thickness of roughly 0.2 mm. SAXS observations were carried out at beamline ID01 of the European Synchrotron Radiation Facility (ESRF). Images obtained from the nanocomposites consisted of isotropic rings and were integrated azimuthally for further analysis. Noise from slits and windows has been subtracted, and statistical errors from the photon flux have also been taken into account in the integration. Measured curves were normalized for variations of the primary intensity. Absolute scattering intensities were calculated from the normalized intensity and film/pellet thickness. The scattering intensity is represented as a function of the modulus of the scattering vector $q = (4\pi/\lambda)\sin\theta$, λ being the wavelength and 2θ being the scattering angle.

3. Results and discussion

3.1. Sample description and SAXS results

Fig. 2 shows the variation of the absolute scattering intensity with q for a nanocomposite sample prepared from stock solution 2, using an iron/polymer molar ratio of 0.11 as described in §2. The curve shows three regions in accordance with reports on granular and mesoporous media (Spalla *et al.*, 2003): (I) a low-q region that follows a power-law regime; (II) an intermediate region that follows a Guinier regime; and (III) a high-q region that also shows a power-law regime. In the inset in Fig. 2, a high-resolution TEM image of a slice of the sample shows isolated spherical particles uniformly distributed in the matrix. A particle population analysis on the TEM images yields a monomodal size distribution with an average particle size $D = 4.5 \pm 0.5$ nm. Fig. 3 shows SAXS log–log plots of as-prepared films and pressed powder pellets of another nanocomposite sample prepared from stock solution 1, using an iron/polymer ratio of 0.04. SAXS curves corre-

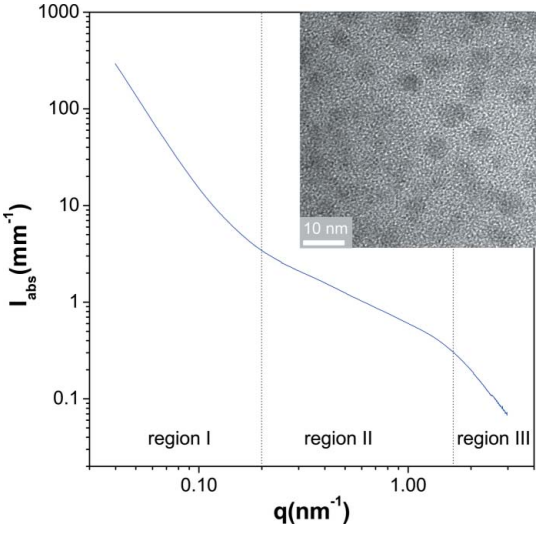

Figure 2
SAXS data of a pellet of a maghemite–poly(4-vinylpyridine) nanocomposite sample containing a 3% volume ratio of spherical particles with $D = 4.5 \pm 0.4$ nm. Vertical lines separate regions of Porod regimes (regions I and III) and a Guinier regime (region II). In the inset a high-resolution electron microscope image of the sample is shown.

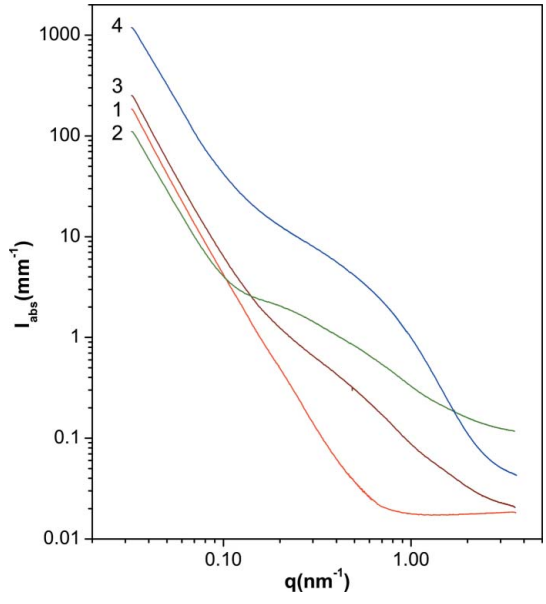

Figure 3
SAXS data of a pure polymer pellet (1), a maghemite–polymer as-prepared nanocomposite film (2), a pellet of the same sample (3), and a pellet made by mixing and pressing polymer and maghemite powders.

Table 1
Characteristics of the nanocomposite samples.

Sample	[Fe]/[PVP]	Particle volume fraction (estimated)	Particle volume fraction (SAXS)	D_{SAXS} (nm)	Estimated interparticle separation (nm)	R_F (nm)
S1	0.032	0.0031	0.0041	1.55	6.99	7.75
S2	0.101	0.0098	0.0066	2.45	6.78	6.07
S3	0.194	0.0186	0.0178	3.49	7.12	6.07
S4	0.391	0.0367	0.0383	5.16	7.35	6.20
S5	0.828	0.0747	0.3820	6.97	6.37	—
S6	1.479	0.1261	0.9067	10.45	6.35	—

sponding to a pure polymer pellet and a pellet prepared by mixing maghemite and polymer powders are also shown in this figure.

All the plots, including those of the pure polymer and the as-prepared film, show a power-law regime in the low-q region ($q < 0.1$ nm^{-1}). Therefore, this scattering intensity must arise from the polymer and is not an artefact introduced during the preparation of the pellet. A fitting of the polymer scattering data to a Porod expression (Porod, 1982),

$$I_{PVP}(q) = I_0 + Aq^{-n}, \tag{1}$$

yields $n = 3.31$, whereas an ideally smooth surface should give $n = 4$, and a Gaussian polymer should give $n = 2$. Thus, this scattering intensity probably comes from the rough surface of grains formed by folded polymer chains.

The polymer SAXS curve shows a constant scattering for $q > 0.1$ nm^{-1}, whereas all curves containing maghemite nanoparticles have enhanced intensities in this region, which is therefore associated with the nanoparticles. In this region, a Guinier and a power-law regime can be discerned.

Series of nanocomposite samples were prepared by the procedure described in §2 using variable iron loadings in the polymer. The iron/poly(4-vinylpyridine) molar ratios used in the preparation of the nanocomposite samples are shown in Table 1. According to XRD observations, the nanocomposites contain maghemite particles of a size that increases with the iron loading used in the sample preparation. As observed in the SAXS curves of the nanocomposites

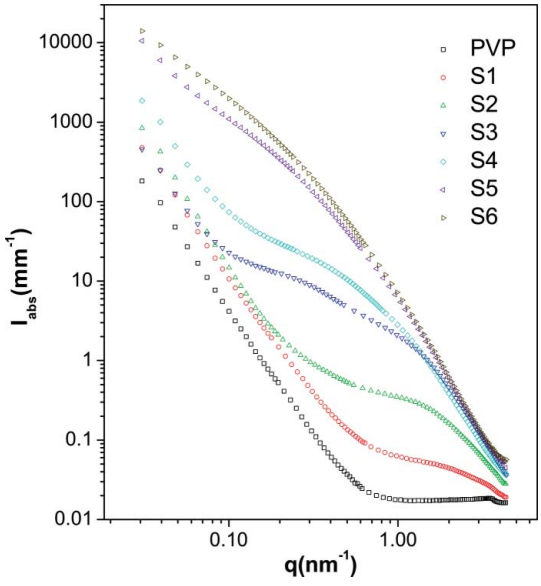

Figure 4
SAXS data of maghemite–PVP nanocomposites prepared from different iron/polymer ratios: 0.032 (S1) 0.101 (S2), 0.194 (S3), 0.391 (S4), 0.828 (S5) and 1.479 (S6).

of Figs. 2 and 3, SAXS curves of these samples (Fig. 4) also show a power law in the low-q region due to the polymer and an enhanced intensity due to the nanoparticles.

This enhanced intensity increases with the iron content, showing an increase of the particles density and/or size. In samples S1 and S2, with low iron content, the nanoparticle scattering shows Guinier and power-law regimes. As the iron content increases, the power law becomes more visible and its exponent approaches −3.60, indicating the existence of particles with rough surfaces. At the same time, as the iron content increases, the transition from the Guinier to the power-law regime occurs at successively lower q values, which gives a qualitative indication of an increase of the particles size. In samples S3 and S4, with intermediate iron content, the nanoparticle scattering also has a 'knee-like' feature at $q \simeq 0.37$ nm^{-1}. This knee-like feature can be due either to a second particle population or to particle aggregates.

3.2. SAXS analysis

As pointed out above, the SAXS intensity of nanocomposites is the sum of the polymer and particle contributions. Polymer scattering is significant in the low-angle region and it can be fitted to equation (1) for all the samples. Regarding particle scattering, two approaches were considered: (i) the existence of a bimodal distribution of nanoparticles and (ii) the existence of a monomodal distribution of nanoparticles and interparticle interactions. The complexity of the system is increased by the fact that the particle size distribution shows a certain dispersion, however low. Consequently, we have used an approximate approach for data analysis. Particle scattering has been considered as a two-electron-density system (Glatter & Kratky, 1982) and has been fitted to a unified equation proposed by Beaucage (1995, 1996),

$$I_p(q) = G_p \exp\left(\frac{R_g^2 q^2}{3}\right) + B_p \left(\frac{\left\{\mathrm{erf}\left[qR_g/\left(6^{1/2}\right)\right]\right\}^3}{q}\right)^p. \tag{2}$$

For a two-electron-density model G_p is defined as

$$G_p = N_p(\rho_p - \rho_m)^2 v_p^2, \tag{3}$$

where N_p is the number of particles, ρ_p and ρ_m are the electron densities of particle and polymer matrix, respectively, v_p is the particle volume, and R_g is the particle radius. For $p = 4$, B_p is the Porod constant defined as

$$B_p = 2\pi(\rho_p - \rho_m)^2 S, \tag{4}$$

where S is the nanoparticle surface area.

The exponential prefactor in the last term of the polymer contribution describes the high-q cut-off for the particle scattering. The Beaucage approach successfully describes scattering from polydispersed nano-objects with different shapes and scattering from multiple-size structures (Beaucage, 1995). From the above expression it is possible to determine the parameters R_g, B_p and G_p, which allows

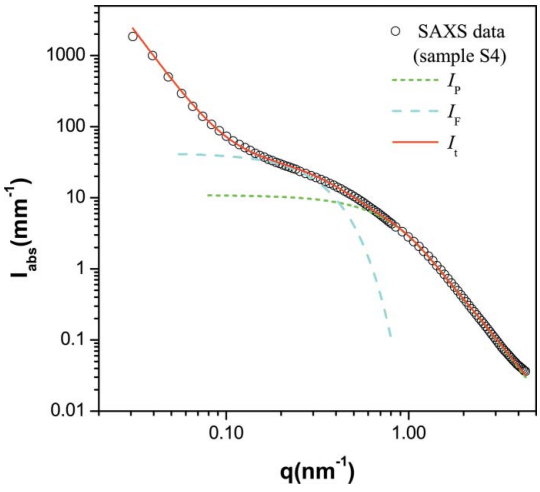

Figure 5
SAXS data of sample S4. Lines correspond to: total fitted intensity (I_t, straight line), particle scattering term (I_P, short-dashed line) and a term attributed in the first instance to a second set of nanoparticles (I_F, dashed line).

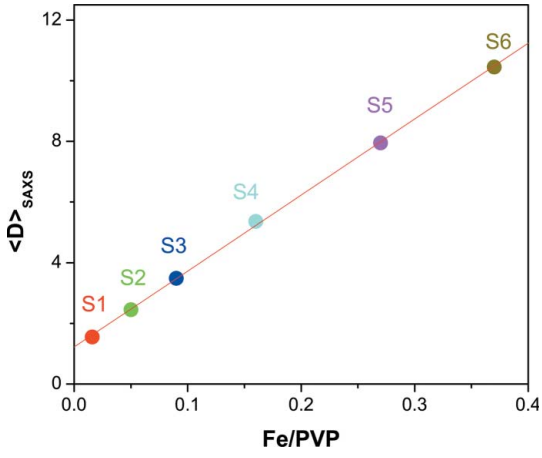

Figure 6
Variation of the calculated particle diameter with the iron mass ratio used in the preparation of the sample.

the mean diameter and the standard deviation of the particle distribution (Beaucage *et al.*, 2004), and the distribution profiles to be calculated. In the samples with higher iron content we have considered another term, $I_F(q)$, similar to that of equation (1),

$$I_F(q) = G_F \exp\left(\frac{R_{gF}^2 q^2}{3}\right) + B_F \left(\frac{\{\mathrm{erf}[qR_{gF}/(6^{1/2})]\}^3}{q}\right)^{p^2}, \quad (5)$$

to describe the above-mentioned 'knee-like' feature as arising from a second set of nanoparticles, so that the total intensity can be expressed as

$$I_t(q) = I_{PVP}(q) + I_p(q) + I_F(q). \quad (6)$$

A representative fitting of this expression to the data from sample S4 is shown in Fig. 5.

The particle average diameters were determined from $\langle D\rangle_{SAXS} = 2(5/3)^{1/2}R_g$ and $R_F = (5/3)^{1/2}R_{gF}$ using R_g and R_{gF} obtained from fitting the SAXS data to equation (6). Particle volume fractions, $\Phi = N_p v_p$, calculated from G_p are also shown in Table 1. As shown in Fig. 6, $\langle D\rangle_{SAXS}$ increases with the iron content, indicating that as the iron loading increases, particles grow larger. For moderate particle densities, Φ is in good accordance with the values calculated from the iron content in the sample and maghemite and PVP densities. However, for large particle volumes, the SAXS volume fraction is clearly exceeding the expected values, indicating an enhanced scattering probably due to a structure contribution. The particle diameter for sample S4 from SAXS (5.2 nm) is in agreement with that obtained from TEM images (6.4 ± 1.1 nm, Fig. 7), with the difference between the values being of the order of the distribution width. This means that the phenomenological Beaucage approach can be used to obtain reliable structural parameters in nanocomposites with multiple-size structures, in accordance with previous results (Beaucage, 1995; Beaucage *et al.*, 2004). The distance R_F associated with the 'knee-like' feature is roughly constant for samples S2–S4 (6.07–6.20 nm) and it increases in sample S1 (7.75 nm) with the lowest iron content.

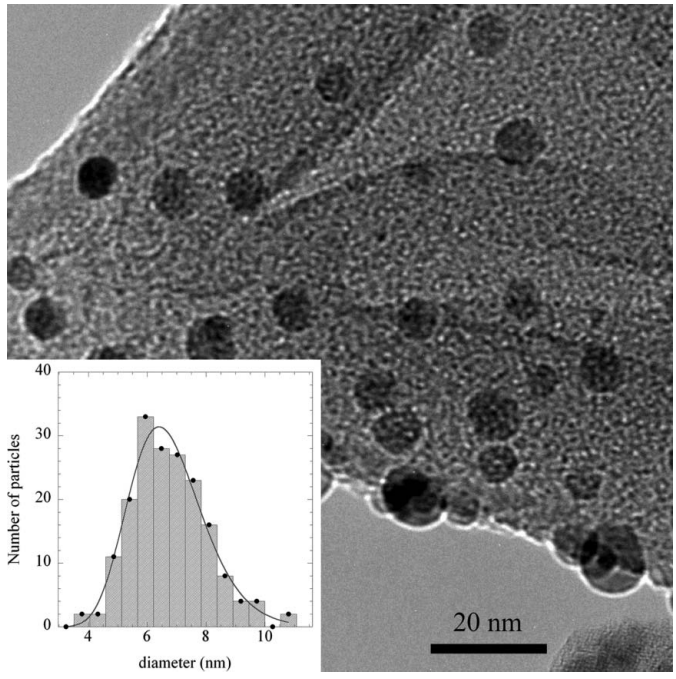

Figure 7
Electron microscope (EM) image of nanocomposite sample S4 dispersed in acetone. At the bottom left the EM size distribution of the sample is shown.

In approach (ii) we have considered the 'knee-like' feature as arising from interparticle interactions with the SAXS intensity being given by

$$I(q) = NP(q)S(q), \quad (7)$$

where $P(q)$ accounts for the particle form factor and $S(q)$ is the structure factor related to interparticle interferences. We studied the presence of interference effects with a Zernike–Prins liquid-like approximation (Riello & Benedetti, 1997), a Born–Green approximation (Riello & Benedetti, 1997; Fournet & Guinier, 1955) assuming a hard-sphere potential interaction, and a distorted one-dimensional lattice (Laity *et al.*, 2004) at the intermediate angle range scattering. However, none of the applied models seem to fit the scattering intensity. In this approach, the 'knee-like' feature corresponds to a smeared maximum corresponding to a characteristic interparticle average distance d that can be estimated as $2\pi/q_{max}$, where q_{max} is the 'knee' position: $d = 20$ and 17 nm for samples S3 and S4, respectively.

In the case of sample S4, the value of R_F is not acceptable as being due to particle size, since it would yield a particle diameter of 12.4 nm, out of the distribution range obtained from TEM. In the case

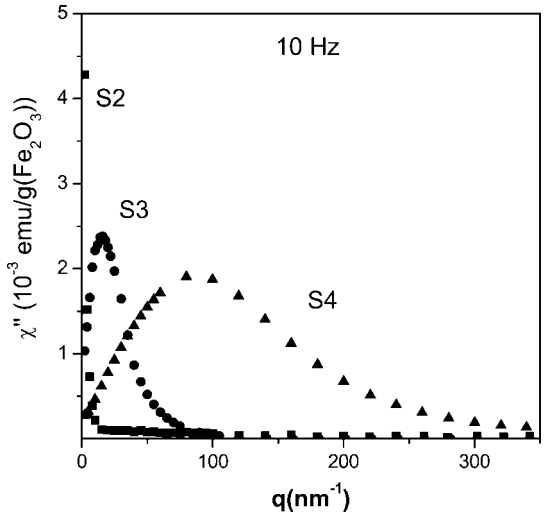

Figure 8
Temperature dependence of the out-of-phase a.c. susceptibility, at 10 Hz, for maghemite nanocomposite samples S2, S3 and S4.

of samples with lower iron content (S1, S2 and S3), R_F is far from $\langle D \rangle_{SAXS}$, and if R_F is a particle radius, the samples shall have a distinct bimodal size distribution. Such marked bimodal size distribution would be also apparent in other properties of the nanocomposites, such as the magnetic susceptibility. It is well known that superparamagnetic nanoparticles yield a signal in the out-of-phase a.c. susceptibility, χ'', *versus* temperature curve that is highly correlated to particle size and shape, and to interparticle interactions. Plots of $\chi''(T)$ for samples S2, S3 and S4 (Fig. 8) show a single peak, which is strong evidence of a monomodal particle population along the whole sample. Moreover, the existence of a second population of maghemite particles with a radius R_F (Table 1) would yield a peak in the susceptibility χ'' around 300 K, a feature that is clearly absent in the curves in Fig. 8. Furthermore, the Gaussian-like shape of the peak is also indicative of the absence of magnetic interactions between particles, and consequently the absence of compact aggregates in the samples. Therefore, the low-angle peak on the scattering intensity profile can not arise from a second population of particles or from dense particle aggregates.

4. Conclusion

We have studied the SAXS profiles of maghemite/polymer nanocomposites containing isolated nanoparticles with a low size dispersion uniformly distributed within the polymer matrix. These profiles have a non-negligible contribution from both the polymer matrix and the nanoparticles, showing two power-law regions and a Guinier region, typical of multiscale structured systems such as granular porous media and nanoparticle composites. The scattering intensity associated with the nanoparticles (a power and a Guinier law) increases with the iron content, as expected for an increase of the size and/or the density of the nanoparticles. In fact, using the Beaucage approach (Beaucage, 1995), we concluded that the particle size increases linearly with the iron content. SAXS curves also show a 'knee-like' feature that could be due to another particle characteristic size or due to interparticle interactions. We present arguments based on magnetic susceptibility and TEM results favouring the latter explanation.

Financial support has been provided by research grant MAT2001-3507-C02-02 from the Spanish CICYT and by the Communauté de Travail des Pirénées. This work has been carried out in the frame of the EC NoE 'MAGMANET'. The ESRF is greatly acknowledged for beamtime allocation. NJOS acknowledges the Portuguese FCT (grant No. SFRH/BD/10383/2002). CQ acknowledges support from the Spanish Government and the European social fund through the 'Ramón y Cajal' program.

References

Beaucage, G. (1995). *J. Appl. Cryst.* **28**, 717–728.
Beaucage, G. (1996). *J. Appl. Cryst.* **29**, 134–146.
Beaucage, G., Kammer, H. K. & Pratsinis, S. E. (2004). *J. Appl. Cryst.* **37**, 523–535.
Bhimani, Z. & Wilson, B. (1997). *Ind. Lubr. Tribol.* **49**, 288–290.
Bogoyevitch, M. A., Kendrick, T. S., Ng, D. C. H. & Barr, R. K. (2002). *DNA Cell Biol.* **21**, 879–894.
Brigger, I., Dubernet, C. & Couvreur, P. (2002). *Adv. Drug Deliver. Rev.* **54**, 631–651.
Brosseau, C., Ben Youssef, J., Talbot, P. & Konn, A. M. (2003). *J. Appl. Phys.* **93**, 9243–9256.
Chin, T. S. (2000). *J. Magn. Magn. Mater.* **209**, 75–79.
Crainic, M. S. & Schlett, Z. (2004). *J. Magn. Magn. Mater.* **268**, 8–19.
Fournet, G. & Guinier, A. (1955). *Small-Angle Scattering of X-rays*. New York: Wiley.
Glatter, O. & Kratky, O. (1982). *Small-Angle Scattering of X-rays*. New York: Academic Press.
Iglesias, O. & Labarta, A. (2001). *Phys. Rev. B*, **63**, 184416(11).
Jordan, A., Scholz, R., Maier-Hauff, K., Johannsen, M., Wust, P., Nadobny, J., Schirra, H., Schmidt, H., Deger, S. & Loening, S. (2001). *J. Magn. Magn. Mater.* **225**, 118–126.
Kamiyama, S., Okamoto, K. & Oyama, T. (2002). *Energ. Convers. Manage.* **43**, 281–287.
Laity, P. R., Taylor, J. E., Wong, S. S., Khunkamchoo, P., Norris, K., Cable, M., Andrews, G. T., Johnson, A. F. & Cameron, R. E. (2004). *Polymer*, **45**, 7273–7291.
Meisen, U. & Kathrein, H. (2000). *J. Imaging Sci. Technol.* **44**, 508–513.
Millan, A., Palacio, F., Falqui, A., Snoeck, E., Serin, V., Bhattacharjee, A., Ksenofontov, V., Gütlich, P. & Gilbert, I. (2007). *Acta Mater.* **55**, 2201–2209.
Mørup, S. & Tronc, E. (1994). *Phys. Rev. Lett.* **72**, 3278–3281.
Porod, G. (1982). *Small-Angle X-ray Scattering*, edited by O. Glatter & O. Kratky, pp. 17–51. New York: Academic Press.
Redl, F. X., Cho, K. S., Murray, C. B. & O'Brien, C. B. (2003). *Nature (London)*, **423**, 968–971.
Riello, P. P. & Benedetti, A. (1997). *J. Chem. Phys.* **106**, 8660–8663.
Safarik, I. & Safarikova, M. (2002). *Monatsh. Chem.* **133**, 737–759.
Schwertmann, U. & Taylor, R. M. (1989). *Minerals in Soil Environments*, edited by J. B. Dixon & S. B. Weed, pp. 379–438. Madison: Soil Sci. Soc. Am.
Spalla, O., Lyonnard, S. & Testard, F. (2003). *J. Appl. Cryst.* **36**, 338–347.
Takafuji, M., Ide, S., Ihara, H. & Xu, Z. H. (2004). *Chem. Mater.* **16**, 1977–1983.
Uhlen, M. (1989). *Nature (London)*, **340**, 733–734.
Veitch, R. J. (2001). *IEEE Trans. Magn.* **37**, 1609–1611.
Weissleder, R. & Papisov, M. (1992). *Rev. Magn. Reson. Med.* **4**, 1–20.